Check for updates

Insulator-to-metal transition of lithium–sulfur battery

Yong Pan, [ID] *[a] Weiming Guan [ID] [b] and Pengyu Mao[a]

Li$_2$S is a promising battery material due to the high theoretical capacity and high energy density. However, the improvement of insulation of Li$_2$S is a challenge for its application. Naturally, the insulator-to-metal transition strongly depends on the electronic overlap between the conduction band and the valence band at the Fermi level (E_F). To solve this key problem, this work investigates the insulator-to-metal transition of Li$_2$S under high pressure. We identify a stable structure based on the phonon dispersion and thermodynamic model. It is found that Li$_2$S with CaF$_2$-type, Br$_2$O-type and Cs$_2$S-type structures are dynamically stable in the ground state. Importantly, the band gap of Li$_2$S decreases gradually with increasing pressure. We predict that pressure leads to the insulator-to-metal transition of Li$_2$S owing to the Li atomic pairing and the existence of Li–Li metallic bonds.

1. Introduction

With increasing global energy consumption and environmental pollution from fossil fuels, energy storage technology becomes an imminent concern both at present and in the future. Lithium–sulfurs (Li–S) are now applied in solid-state secondary batteries.[1–6] In particular, the theoretical capacity and theoretical specific energy of lithium–sulfurs are up to 1675 mA h g^{-1} and 2600 W h kg^{-1}, respectively.[7,8] However, the insulating nature of lithium–sulfur markedly reduces the electrochemical reaction dynamics and weakens the overall energy efficiency due to the low Li-ion diffusivity rate.[9–11] Importantly, the insulation of lithium–sulfurs reduces the polarization and aggravates cell impedance, which reduces the electrical transportation and energy rate of a cell. As a result, these factors further degrade the performance of a battery, cycle life, safety *etc.* Therefore, the improvement of the electrical properties of lithium–sulfur batteries is a key challenge for their practical application.

Earlier work has shown that the obtained indirect band gap of Li$_2$S with CaF$_2$-type structure is about 3.297 eV.[12] One viewpoint is that the insulating nature of Li$_2$S is attributed to the Li–S bonding and insulation of pure S.[13,14] Essentially, the insulating nature of Li$_2$S derives from the formation of a wide band gap. That is to say, it is difficult to induce an electronic transition between the bottom of the conduction band and the top of the valence band. The insulator-to-metal transition of a solid strongly depends on the localized hybridization at the

Fermi level (E_F).[15] To solve this key problem, it is necessary to improve the electronic overlap at the Fermi level. Based on the above design principle, we propose that pressure may lead to insulator-to-metal transition of Li$_2$S.

The electrochemical reaction of crystalline α-S8 at a cathode is described by: S8 + 16Li$^+$ + 16e$^-$ ↔ 8Li$_2$S.[16] Although the structure, electronic structure and elastic properties of Li$_2$S have been studied,[12,17] it is extremely unstable in air because of strong moisture absorption.[18,19] Therefore, structural stability plays a crucial role in overall performance such as electrical properties, rate performance, rapid capacity fade, cycle life, safety *etc.* For the Li$_2$S compound, there are three different structures: CaF$_2$-type structure,[20] Br$_2$O-type structure[21] and Na$_2$S-type structure.[21] However, the structural stability of Li$_2$S at high pressure is unknown.

To explore the insulator-to-metal transition, in this work, we apply first-principles calculations within the density functional theory (DFT) method to investigate the correlation between pressure and properties of Li$_2$S (0–350 GPa). Considering the structural features and phase stability under high pressure, we design five possible crystal structures based on main group elements. The structural stability of these structures is examined by the thermodynamic mode and phonon dispersion. Our works predict that high pressure can result in insulator-to-metal transition of Li$_2$S.

2. Model and method

To confirm the stable structure under high pressure, we designed five possible crystal structures, namely CaF$_2$-type (space group: $Fm\bar{3}m$, no. 225),[20] Br$_2$O-type (space group: $Pn21a$, no. 33),[21] Na$_2$S-type (space group: $P6_3/mmc$, no. 194),[22] K$_2$S-type (space group: $Pmma$, no. 51)[12,23] and Cs$_2$S-type (space group:

[a]School of Material Science and Engineering, Southwest Petroleum University, Chengdu 610500, China. E-mail: panyong10@mails.jlu.edu; Fax: +86-871-68438950; Tel: +86-871-68328970

[b]State Key Laboratory of Advanced Technologies for Comprehensive Utilization of Platinum Metals, Kunming 650106, China

Pnma, no. 62),[21] because of their similar structural features. The structural models of Li_2S are shown in Fig. 1. Generally speaking, the structural stability of a solid is measured by thermodynamic and dynamic models. In particular, the dynamic stability of a solid is related to the vibrational frequency, which is defined as the phonon frequency.

It is well known that the first-principles calculation within DFT is a strong tool to predict a new crystal structure at the electronic or atomic level.[24] In this paper, therefore, all calculations of the five Li_2S structures at zero pressure and high pressure were carried out by using first-principles calculations, as implemented in the CASTEP code.[25] After convergence test, we selected the generalized gradient approximation (GGA) within PBE[26] functional and the local density approximation (LDA) within CA-PZ functional[27] to treat the electronic interaction and for comparison. The interaction between the ionic cores and valence electrons was treated using the ultrasoft pseudopotential. The valence electronic configurations of Li and S are $1s^2 2s^1$ and $3s^2 3p^4$, respectively. To ensure the total energy in the ground state to be converged, a plane-wave basis set for electron wave functions with cutoff energy of 400 eV was used. The Brillouin zone was sampled with $14 \times 14 \times 14$, $9 \times 14 \times 9$, $14 \times 14 \times 14$, $9 \times 10 \times 9$ and $9 \times 14 \times 9$ for CaF_2-type structure, Br_2O-type structure, Na_2S-type structure, K_2S-type structure and Cs_2S-type structure, respectively. The electronic energy tolerance of the SCF was treated as 1×10^{-6} eV per atom. Total energy of a system was obtained by the density-mixing scheme in conjunction with the conjugate gradient technique. The Broyden–Fletcher–Goldfarb–Shanno (BFGS) algorithm was applied to treat the relaxed system. All structures were optimized based on the periodic boundary condition. Note that all atomic positions, lattice parameters and internal coordinates in a system were fully relaxed. To estimate the dynamical stability, the phonon properties were calculated by using the PHONOPY code.[28,29]

3. Results and discussion

It is obvious that the assessment of structural stability of Li_2S should be studied first. Essentially, the structural stability of a solid relies not only on the chemical potential between atoms but also on the vibrational frequency. Therefore, we consider the structural stability of Li_2S from two aspects: thermodynamic and dynamic stabilities. The thermodynamic stability of Li_2S is calculated by the formation enthalpy (ΔH), which is given by:

$$\Delta H = E(Li_2S) - 2E(Li) - E(S) \tag{1}$$

Table 1 Calculated lattice parameters a-axis, b-axis and c-axis (Å), volume, V (Å^3), formation enthalpy, ΔH (eV per atom), and bulk modulus, B (GPa), of Li_2S with five structures

Structure	Method	a	b	c	V	ΔH	B
CaF_2-type	Cal	5.725			187.6	−4.0161	38
	Exp[20]	5.720					
Na_2S-type	Cal	4.043		6.071	86.0	−3.8846	36
K_2S-type	Cal	6.076	4.041	7.011	172.2	−3.8847	37
Cs_2S-type	Cal	6.326	3.818	7.281	185.9	−3.9578	39
Br_2O-type	Cal	11.463	4.046	4.049	187.8	−4.0148	37
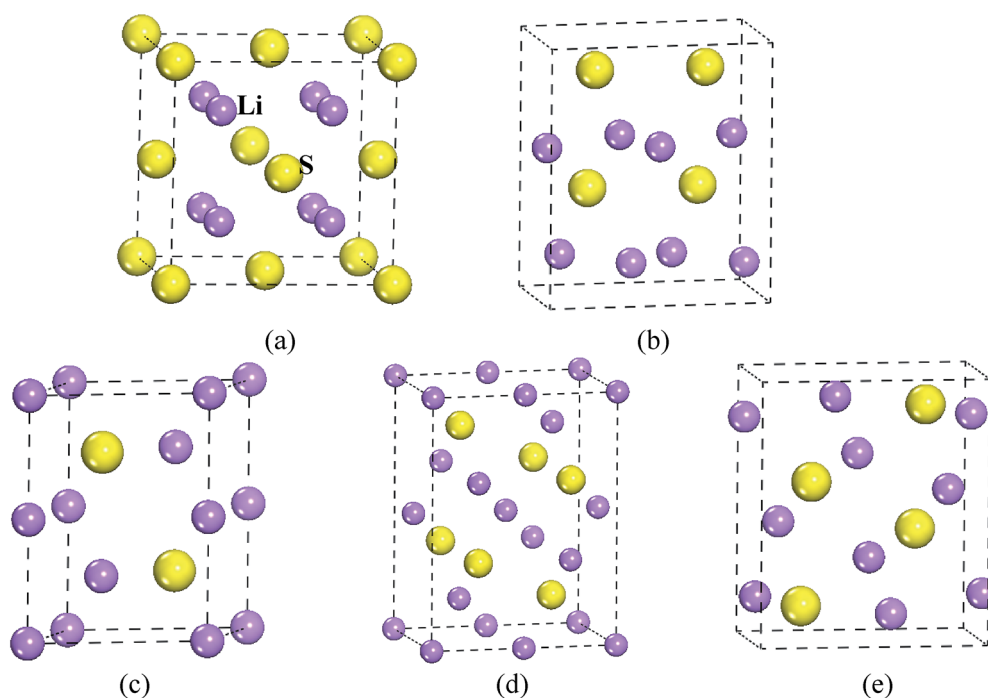
Fig. 1 Structural model of Li_2S. (a) CaF_2-type structure, (b) Br_2O-type structure, (c) Na_2S-type structure, (d) K_2S-type structure and (e) Cs_2S-type structure.
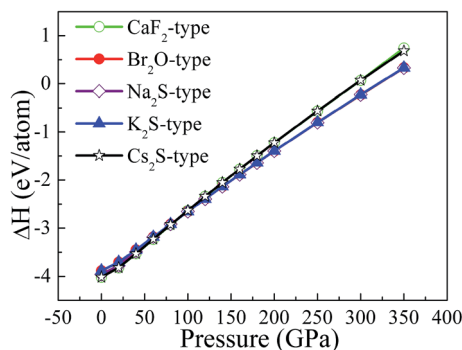
Fig. 2 The calculated formation enthalpy of Li_2S with increasing pressure between 0 and 350 GPa.

where $E(Li_2S)$, $E(Li)$ and $E(S)$ are the total energy of Li_2S, Li atom and S atom in the ground state.

Table 1 presents the calculated lattice parameters, volume, formation enthalpy and bulk modulus of Li_2S with the five structures. It can be seen that the calculated formation enthalpy of these structures is smaller than zero, indicating that these structures are thermodynamically stable in the ground state. Importantly, the calculated formation enthalpy of Li_2S with CaF_2-type structure is about -4.0161 eV per atom, which is smaller than that of the other structures. That is to say, Li_2S with CaF_2-type structure is more thermodynamically stable than the other structures. This result is in good agreement with other theoretical results.[16]

To reveal the thermodynamic stability, the structural formation and chemical bonding of Li_2S are discussed here. As presented in Table 1, the calculated lattice parameter of Li_2S with CaF_2-type structure is $a = 5.725$ Å, which is in good agreement with the experimental data.[20] It is clear that the structural stability of the CaF_2-type structure is attributed to the symmetrical Li and S atoms. As shown in Fig. 1, Li and S atoms occupy the Wyckoff 8c (0.250, 0.2500, 0.500) and 4a (0, 0, 0) sites, respectively, which form the symmetrical Li–S bond and Li–Li metallic bond. The calculated bond lengths of Li–S bond and Li–Li metallic bond are 2.479 Å and 2.863 Å, respectively, which are in good agreement with other theoretical results.[30,31] The symmetrical atomic configuration can effectively improve the structural stability of Li_2S.

However, the structural features of the other four structures are different from those of the CaF_2-type structure. From Fig. 1,

we can see that Br_2O-type, K_2S-type and Cs_2S-type belong to the orthorhombic structure, and Na_2S-type is a hexagonal structure. Therefore, the atomic configuration of these structures is different from that of the CaF_2-type structure. As presented in Table 1, the calculated value of the b-axis of Na_2S-type, K_2S-type, Cs_2S-type and Br_2O-type is smaller than the corresponding axis for CaF_2-type. It is worth noticing that the calculated a-axis (except for Na_2S-type) and c-axis (except for Br_2O-type) of those predicted structures are larger than the corresponding axes for CaF_2-type structure. The calculated volume of Br_2O-type structure is slightly larger than that of CaF_2-type structure. On the contrary, the calculated volume of Na_2S-type, K_2S-type and Cs_2S-type is smaller than that of CaF_2-type structure. These results indicate that the symmetrical atomic arrangement of these predicted structures is weaker than that of CaF_2-type structure. As a result, the localized hybridization between atoms of the former is weaker than that of CaF_2-type structure. This is why the thermodynamic stability of the CaF_2-type structure is better than that of the other predicted structures.

To study the influence of pressure on the structural stability of Li_2S, Fig. 2 displays the calculated formation enthalpy of Li_2S as a function of pressure. In particular, we examine the phase transition of Li_2S (0–350 GPa). For Li_2S, high pressure markedly improves the coulomb repulsion between Li atom and S atom, which results in a large chemical potential. As a result, the formation enthalpies of Li_2S with the five structures increase monotonically with increasing pressure. From Fig. 2, it is observed that the calculated formation enthalpy of Li_2S increases with increasing pressure. We suggest that this trend is attributed to the variation of electronic structure under pressure. To reveal the nature of formation enthalpy under pressure, Fig. 3 shows the calculated unit-cell volume and chemical bonding of Li_2S with the five structures. Here, we consider the bond length of Li–S bond and Li–Li metallic bond under high pressure. It is clear that the calculated unit-cell volume and bond lengths of Li_2S decrease gradually with increasing pressure. In other words, high pressure can increase the coulomb repulsion between Li atom and S atom. This is why the formation enthalpy of Li_2S monotonically increases under pressure.

Importantly, we further find that pressure leads to a phase transition from CaF_2-type structure to Na_2S-type structure at $\sim$100 GPa (see Fig. 2) because the calculated formation enthalpy of CaF_2-type structure is slightly smaller than that of Na_2S-type structure when the pressure is below 100 GPa. On the contrary, the calculated formation enthalpy of CaF_2-type structure is
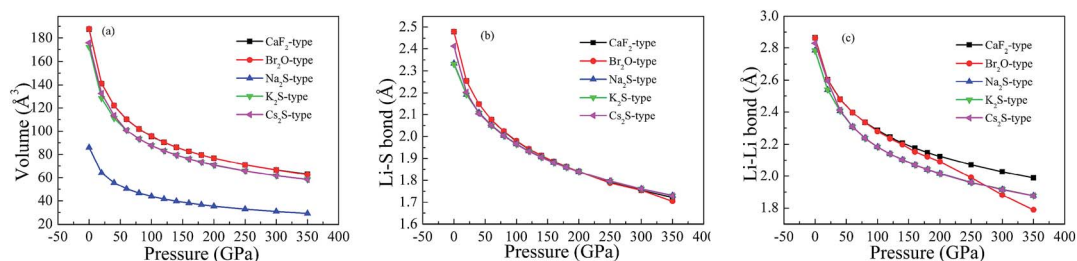

Fig. 3 The calculated (a) volume and (b and c) bond lengths of Li_2S as a function of pressure.

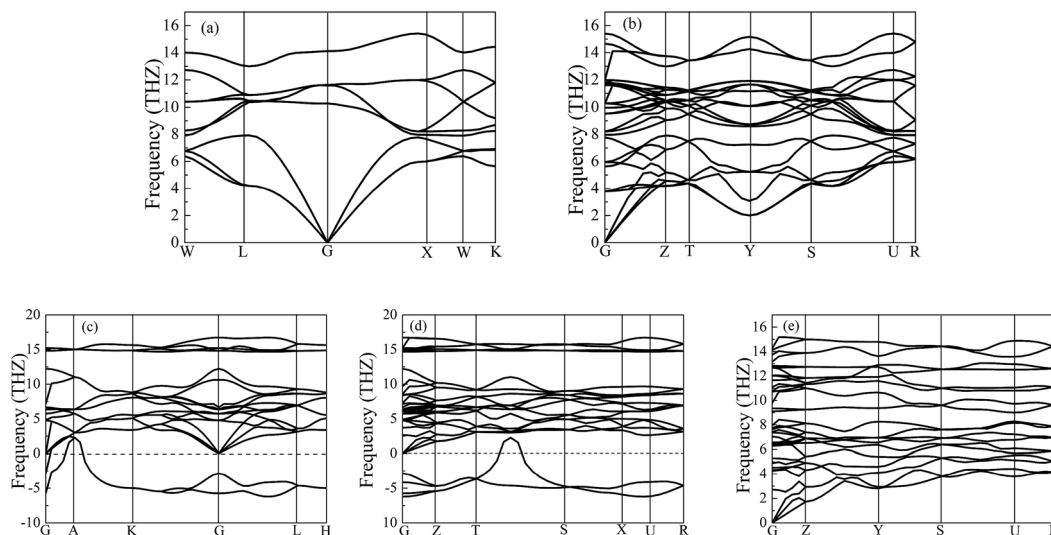**Fig. 4** Calculated phonon dispersion curves of Li$_2$S at 0 GPa. (a) CaF$_2$-type structure, (b) Br$_2$O-type structure, (c) Na$_2$S-type structure, (d) K$_2$S-type structure and (e) Cs$_2$S-type structure.

bigger than that of Na$_2$S-type structure when the pressure is above 100 GPa. This discrepancy is demonstrated by the lattice parameters and chemical bonding. For CaF$_2$-type structure, the lattice parameter decreases with increasing pressure. In particular, pressure results in charge transfer from Li–S to Li–Li atoms. Although the trend of lattice parameters of Na$_2$S-type structure is similar to that of CaF$_2$-type structure, the coulomb repulsion of Li–Li atoms of Na$_2$S-type structure is less than that of the corresponding atoms for CaF$_2$-type structure. This discrepancy can give rise to a phase transition under high pressure.

Importantly, the dynamical stability of a solid is related to the phonon frequency,[32,33] which is calculated by the phonon dispersion. Generally speaking, imaginary phonon frequency

indicates dynamical instability. On the contrary, no imaginary phonon frequency implies dynamical stability in the ground state. To examine the influence of pressure on dynamical stability of Li$_2$S with the five structures, Fig. 4 and 5 present the calculated phonon dispersion curves of Li$_2$S at 0 and 100 GPa, respectively. It can be seen that no imaginary frequencies are observed for CaF$_2$-type structure at 0 and 100 GPa, implying that Li$_2$S with CaF$_2$-type structure is dynamically stable in the ground state. It is obvious that Li$_2$S still retains the CaF$_2$-type structure under high pressure.

On the other hand, our predicted Cs$_2$S-type structure is dynamically stable at zero pressure because no imaginary phonon frequency is found at 0 GPa. On the contrary, Cs$_2$S-type structure is dynamically unstable at 100 GPa because we observe
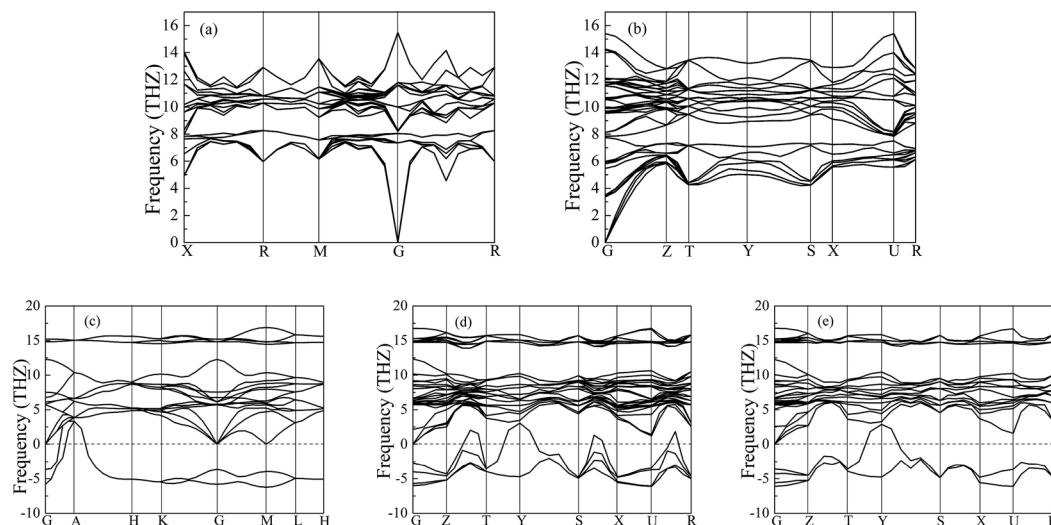

Fig. 5 Calculated phonon dispersion curves of Li$_2$S at 100 GPa. (a) CaF$_2$-type structure, (b) Br$_2$O-type structure, (c) Na$_2$S-type structure, (d) K$_2$S-type structure and (e) Cs$_2$S-type structure.
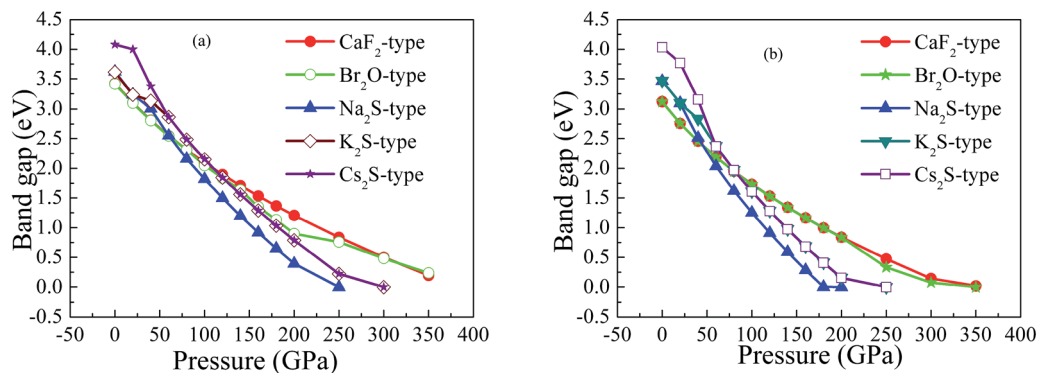
Fig. 6 Band gap of Li$_2$S as a function of pressure: (a) GGA; (b) LDA.
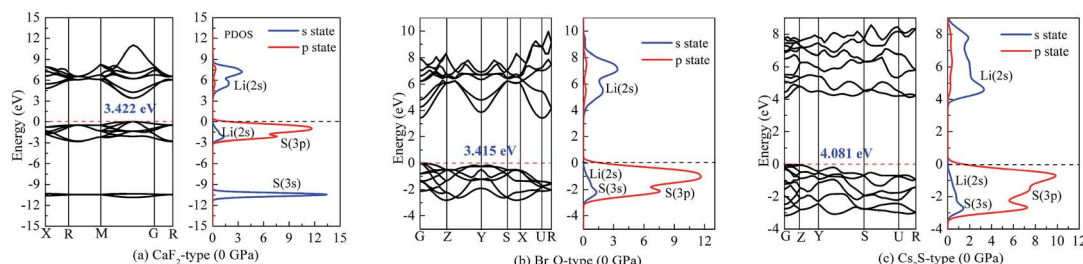
Fig. 7 Band structure and partial density of states (PDOS) at 0 GPa: (a) Li$_2$S with CaF$_2$-type structure, (b) Li$_2$S with Br$_2$O-type structure, (c) Li$_2$S with Cs$_2$S-type structure.

imaginary phonon frequency in this structure when pressure is up to 100 GPa. The dynamical stability of Br$_2$O-type structure is similar to that of CaF$_2$-type structure. It is worth noticing that Li$_2$S with Na$_2$S-type and K$_2$S-type structures are dynamically unstable. To investigate the influence of pressure on the electronic properties, Fig. 6 displays the band gap of Li$_2$S as a function of pressure. In particular, to further examine the electronic properties under high pressure, we consider and compare the GGA functional and LDA functional. It can be seen that the calculated band gap of Li$_2$S with CaF$_2$-type structure is about 3.422 eV by GGA and 3.120 eV by LDA, which are in excellent agreement with other theoretical results (3.297 eV).[12] In addition, the band gap of Cs$_2$S-type structure (4.081 eV by GGA and 4.035 eV by LDA) is larger than that of the other structures. These results demonstrate the insulating nature of Li$_2$S. With increasing pressure, the band gap of the five

structures decreases. Importantly, we find that the value of the band gap is close to zero when pressure is up to 350 GPa. That is to say, high pressure can result in electronic overlap between the bottom of the conduction band and the top of the valence band, which induces an electronic transition between conduction band and valence band. In particular, pressure can improve the charge overlap of atoms with further increasing pressure. As mentioned above, we can conclude that pressure gives rise to insulator-to-metal transition of Li$_2$S.

To understand the nature of the insulator-to-metal transition, Fig. 7 and 8 show the calculated band structure and partial density of states of Li$_2$S at 0 and 350 GPa, respectively. Considering the structural stability, we select the Ca$_2$F-type structure, Br$_2$O-type structure and Cs$_2$S-type structure. The calculated results of band structure at both 0 GPa and 350 GPa are shown for comparison. At 0 GPa, it is clear that the profile of
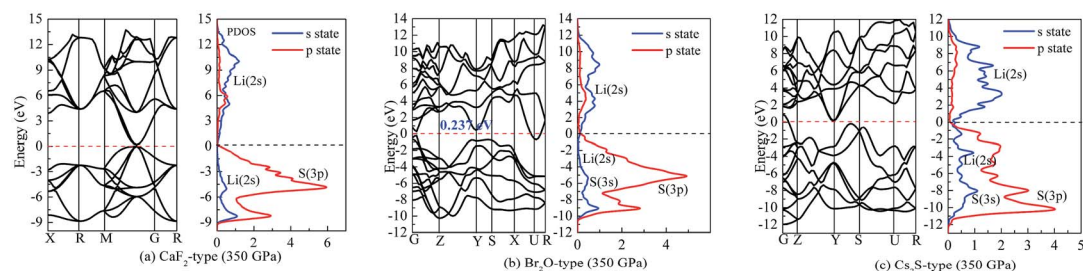

Fig. 8 Band structure and partial density of states (PDOS) at 350 GPa: (a) Li$_2$S with CaF$_2$-type structure, (b) Li$_2$S with Br$_2$O-type structure, (c) Li$_2$S with Cs$_2$S-type structure.

the valence band is mainly contributed by S-3p state and part of Li-2s state. The localized hybridization between S-3p state and Li-2s state forms the Li–S bond. However, the profile of the conduction band mainly derives from Li-2s state. The delocalization of electron acceptor, especially for the position of Li-2s state, determines the degree of charge interaction between the conduction band and valence band.

We assume that pressure can give rise to electronic transport of Li atoms from conduction band to Fermi level. This enhances the localized hybridization between Li-2s state and S-3p state. From Fig. 7, the band width of Li_2S becomes narrow with increasing pressure. We further find an electronic overlap at the Fermi level when pressure is up to 350 GPa. As a result, pressure results in insulator-to-metal transition of Li_2S. We suggest that the main reason is the pairing of Li atoms, especially for 2s-2s localized hybridization of Li atoms. The calculated bond length of Li–Li metallic bond is 1.990 Å. In fact, the electronic overlap is also demonstrated by lattice parameters and chemical bonding. With increasing pressure, the lattice parameters and chemical bonding of the five structures decrease. For example, the calculated lattice parameter of Li_2S with CaF_2-type structure at 0 GPa is $a = 5.725$ Å. However, this lattice parameter decreases to 3.978 Å at 350 GPa.

4. Conclusions

In conclusion, we have investigated the influence of pressure on the structure and insulator-to-metal transition of Li_2S by using first-principles calculations. Five possible crystal structures are examined according to the phonon dispersion and thermodynamic model. Li_2S with CaF_2-type structure is more thermodynamically stable than with the other structures. The calculated phonon dispersions show that Li_2S with CaF_2-type, Br_2O-type and Cs_2S-type structures are dynamically stable in the ground state. However, Li_2S with Na_2S-type and K_2S-type structures are dynamically unstable. The calculated results show that the structural stability of Li_2S derives from the localized hybridization between Li atom and S atom. However, the Li–Li antibonding is the origin of the insulating state for Li_2S. These structures exhibit an insulating nature in the ground state. With increasing pressure, the band width of the five structures decreases and the lattice parameters of these structures decrease. They lead to Li-2s orbital migrating from conduction band to valence band, and to increasing electronic overlap. Our results predict that pressure can result in insulator-to-metal transition of Li_2S.

Conflicts of interest

There are no conflicts to declare.

Acknowledgements

References

1 P. G. Bruce, S. A. Freunberger, L. J. Hardwick and J. M. Tarascon, *Nat. Mater.*, 2012, **11**, 19–29.

2 L. C. H. Gerber, P. D. Frischmann, F. Y. Fan, S. E. Doris, X. Qu, A. M. Scheuermann, K. Persson, Y. M. Chiang and B. A. Helms, *Nano Lett.*, 2016, **16**, 549–554.

3 K. Wang, K. Jiang, B. Chung, T. Ouchi, P. J. Burke, D. A. Boysen, D. J. Bradwell, H. Kim, U. Muecke and D. R. Sadoway, *Nature*, 2014, **514**, 348–350.

4 M. T. Mcdowell, Z. Lu, K. J. Koski, J. H. Yu, G. Zheng and Y. Cui, *Nano Lett.*, 2015, **15**, 1264–1271.

5 Y. Cheng, A. Nie, Q. Zhang, L. Y. Gan, R. S. Yassar and U. Schwingenschlgol, *ACS Nano*, 2014, **8**, 11447–11453.

6 Y. Pan and W. Guan, *Int. J. Hydrogen Energy*, 2016, **41**, 11033–11041.

7 G. Ma, Z. Wen, J. Jin, M. Wu, X. Wu and J. Zhang, *J. Power Sources*, 2016, **267**, 542–546.

8 H. Nagata and Y. Chikusa, *J. Power Sources*, 2016, **329**, 268–272.

9 C. Barchasz, J. C. Lepretre, F. Alloin and S. Patoux, *J. Power Sources*, 2012, **199**, 322–330.

10 J. Liu, H. Nara, T. Yokoshima, T. Momma and T. Osaka, *J. Power Sources*, 2015, **273**, 1136–1141.

11 X. Meng, D. J. Comstock, T. T. Fister and J. W. Elam, *ACS Nano*, 2014, **10**, 10963–10972.

12 R. D. Eithiraj, G. Jaiganesh, G. Kalpana and M. Rajagopalan, *Phys. Status Solidi B*, 2007, **244**, 1337–1346.

13 A. Sakuda, A. Hayashi and M. Tatsumisago, *Sci. Rep.*, 2013, **3**, 2261.

14 S. Urbonaite and P. Novak, *J. Power Sources*, 2014, **249**, 497–502.

15 M. T. Winkler, D. Recht, M. J. Sher, A. J. Said, E. Mazur and M. J. Aziz, *Phys. Rev. Lett.*, 2011, **106**, 178701.

16 H. Park, H. S. Koh and D. J. Siegel, *J. Phys. Chem. C*, 2015, **119**, 4675–4683.

17 H. Khachai, R. Khenata, A. Bouhemadou, A. H. Reshak, A. Haddoou, M. Rabah and B. Soudini, *Solid State Commun.*, 2008, **147**, 178–182.

18 H. Noh, J. Song, J. K. Park and H. T. Kim, *J. Power Sources*, 2015, **293**, 329–335.

19 C. Wang, X. Wang, Y. Yang, A. Kushima, J. Chen, Y. Huang and J. Li, *Nano Lett.*, 2015, **15**, 1796–1802.

20 P. T. Cunningham, S. A. Johnson and E. J. Cairns, *J. Electrochem. Soc.*, 1979, **119**, 1448–1450.

21 A. Grzechnik, A. Vegas, K. Syassen, I. Loa, M. Hanfland and M. Jansen, *J. Solid State Chem.*, 2000, **154**, 603–611.

22 A. Vegas, A. Grzechnik, K. Syassen, I. Loa, M. Hanfland and M. Jansen, *Acta Crystallogr., Sect. B: Struct. Sci.*, 2001, **57**, 151–156.

23 A. Vegas, A. Grzechnik, M. Hanfland, C. Muhle and M. Jansen, *Solid State Sci.*, 2002, **4**, 1077–1081.

24 J. Sun, R. C. Remsing, Y. Zhang, Z. Sun, A. Ruzsinszky, H. Peng, U. Waghmare, X. Wu, M. L. Klein and J. P. Perdew, *Nat. Chem.*, 2016, **8**, 831–836.

25 M. D. Segall, P. J. D. Lindan, M. J. Probert, C. J. Pickard, P. J. Hasnip, S. J. Clark and M. C. Payne, *J. Phys.: Condens. Matter*, 2002, **14**, 2717–2744.

26 G. Kresse and J. Furthmüller, *Phys. Rev. B: Condens. Matter Mater. Phys.*, 1996, **54**, 11169–11186.

27 D. M. Ceperley and B. J. Alder, *Phys. Rev. Lett.*, 1980, **45**, 566–569.

28 K. Kaasbjerg, K. S. Thygesen and K. W. Jacobsen, *Phys. Rev. B: Condens. Matter Mater. Phys.*, 2012, **85**, 115317.

29 Y. Pan and W. Guan, *J. Power Sources*, 2016, **325**, 246–251.

30 Z. Liu, S. Bertolini, P. B. Balbuena and P. P. Mukherjee, *ACS Appl. Mater. Interfaces*, 2016, **8**, 4700–4708.

31 Y. S. Su and A. Manthiram, *Nat. Commun.*, 2012, **3**, 1166.

32 Y. Zhang, V. Ozolins, D. Morelli and C. Wolverton, *Chem. Mater.*, 2014, **26**, 3427–3435.

33 Y. Liu, D. Duan, X. Huang, F. Tian, D. Li, X. Sha, C. Wang, H. Zhang and T. Cui, *J. Phys. Chem. C*, 2015, **119**, 15905–15911.